P1.90 DYNAMICAL SYSTEM ANALYSIS OF A LOW ORDER TROPICAL CYCLONE MODEL

Daria Schönemann and Thomas Frisius[1]
JRG Dynamical Systems, KlimaCampus, Universität Hamburg

1. INTRODUCTION

A tropical cyclone can be considered in an idealized sense as an autonomous dynamical system. Although it is possible to simulate tropical cyclones in numeric models quite accurately, only little is known about their dynamical system characteristics. These characteristics are important in order to find out how often tropical cyclones appear and which intensity they may reach under different climate conditions. Emanuel and Nolan (2004) hypothesized that tropical cyclones can be understood as a stable branch occurring after a subcritical saddle node bifurcation at a certain sea surface temperature. It remains, however, unclear why such a bifurcation should occur and what physical processes are responsible for this. Our aim is to gain more understanding of the dynamical system tropical cyclone by using a hierarchy of models. In this contribution we start with a highly simplified low order model that is lucid enough to grasp its dynamics. It is found that the model indeed reproduces the subcritical bifurcation hypothesized by Emanuel and Nolan (2004).

2. MODEL FORMULATION

The model is based on the assumption of an axisymmetric vortex and is formulated in cylindrical coordinates. The tropical cyclone is divided into three regions above the boundary layer: i) eye, ii) eyewall and iii) outer region (see Fig. 1). The eye is presumed to be at rest with a fixed outer radius. An angular momentum surface forms the boundary between eyewall and outer region. At lower tropospheric levels within the Ekman layer it is located at the radius of maximum winds (RMW). Idealized axisymmetric model simulations reveal that the angular momentum at the RMW remains roughly constant during tropical cyclogenesis (Frisius 2006). For the model formulation it is useful to introduce the so-called potential radius:

$$R = \sqrt{r^2 + 2vr/f} = \sqrt{2m/f}\ , \qquad (1)$$

where r denotes the physical radius, v the tangential velocity, f the Coriolis parameter and m the angular momentum density. We may interpret the model as a box-model since the boundaries between the three regions are fixed in potential radius space.

2.1 THE BOUNDARY LAYER FLOW

The dynamical equations are subject to the hydrostatic and the Boussinesq approximations. The latter leads to non-divergence of the radial-axial flow, i.e.:

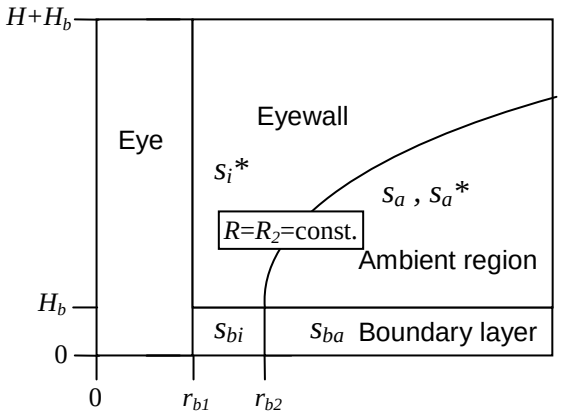

Figure 1: Sketch of the low-order tropical cyclone model.

$$\frac{1}{r}\frac{\partial}{\partial r}(ru) + \frac{\partial w}{\partial z} = 0\ , \qquad (2)$$

where u is the radial velocity, w the vertical velocity and z the height. Because of non-divergence we can introduce a mass-stream function ψ having the following properties:

$$2\pi\, r\rho_b u = -\frac{\partial \psi}{\partial z}, \qquad 2\pi\, \mathrm{r}\rho_b w = \frac{\partial \psi}{\partial r}, \qquad (3)$$

where ρ_b denotes the uniform density in the boundary layer.

The boundary layer is of a constant height H_b. We adopt the simple balanced boundary model of Schubert and Hack (1983) in which a simplified aerodynamic drag law as a function of the balanced tangential wind at the boundary layer top ($z=H_b$) is assumed. By using this closure and vertical integration of the continuity equation (2) we obtain the vertical velocity w_b at $z=H_b$. A comparison to equation (3) leads to the following expression for the

[1] *Corresponding author address:* Thomas Frisius, Junior Research Group Dynamical Systems, KlimaCampus, Universität Hamburg, Grindelberg 5, 20144 Hamburg, Germany;
E-mail: Thomas.Frisius@zmaw.de

mass stream function at the top of the boundary layer:

$$\psi_b = 2\pi\rho_b r_b C_D \frac{|v_b| v_b}{\zeta_b}, \qquad (4)$$

where C_D is the surface drag coefficient and ζ the absolute vorticity. The index b symbolizes evaluation at $z=H_b$. We are aware of the limitations of this simple balanced boundary layer model (see Smith and Montgomery 2008) but think it is appropriate in the context of a low order model. A more accurate closure by incorporation of radial wind in the drag law will be considered in the near future.

2.2 THE EYEWALL

Within the eyewall we assume validity of the gradient wind balance, saturated pseudoadiabatic ascent and angular momentum conservation. These conditions allow for application of the thermal wind balance equation derived by Emanuel (1986) which relates specific saturation entropy s^* to angular momentum density m:

$$\frac{T_b - T}{m}\frac{ds^*}{dm} = \frac{2(T_b - T)}{f^2 R^3}\frac{ds^*}{dR} = \frac{1}{r^2} - \frac{1}{r_b^2}, \qquad (5)$$

where T denotes the temperature. Note that the saturation entropy s* is only a function of angular momentum m. In Eq. (5), the radius r as well as the temperature T, are considered as a function of potential radius R and height z. This equation is evaluated at the outer eyewall boundary where the potential radius takes the value $R=R_2$. The radial gradient of s^* is approximated by a finite difference expression

$$\left.\frac{ds^*}{dR}\right|_{R=R_2} = \frac{s_a^* - s_i^*}{\Delta R}, \qquad (6)$$

where s_i^* and s_a^* are the mean saturation entropies of the eyewall region and the ambient region, respectively. As a model parameter, ΔR represents the potential radial distance between both regions. We approximate that temperature decreases vertically with a constant lapse rate Γ. So we obtain at $R=R_2$:

$$G_2(z - H_b) = \frac{1}{r_2(z)^2} - \frac{1}{r_{b2}^2}, \qquad \text{with } G_2 = \frac{2\Gamma}{f^2 R_2^3}\frac{s_a^* - s_i^*}{\Delta R}. \qquad (7)$$

The index 2 indicates evaluation at the outer eyewall boundary and $r_2(z)$ denotes the physical radius of the angular momentum surface at $R=R_2$. Eq. (7) prescribes the shape of the angular momentum surface at the outer eyewall boundary. However, this equation has two unknowns, namely r_2 and r_{b2}. For a closure we assume that the mass M enveloped by this angular momentum surface is conserved. Using the simplifying assumption that density ρ is a constant (Boussinesq approximation) the mass M as a function of G_2 and r_{b2} becomes[2]

$$M = \pi\rho \int_{H_b}^{H+H_b} r_2^2 dz = \frac{\pi\rho}{G_2}\ln\left\{1 + G_2 r_{b2}^2 H\right\}. \qquad (8)$$

With this relation we can determine the physical radius r_{b2} and tangential wind speed v_{b2} at the outer eyewall boundary by the following equations:

$$r_{b2} = \sqrt{\frac{1}{G_2 H}\left[\exp\left(\frac{G_2 M}{\pi\rho}\right) - 1\right]}, \qquad (9)$$

$$v_{b2} = \frac{f}{2}\frac{R_2^2 - r_{b2}^2}{r_{b2}}. \qquad (10)$$

2.3 THE AMBIENT REGION

Pseudoadiabatic ascent with angular momentum conservation does not take place in the ambient region, which might be partially sub-saturated. The mean specific entropy s_a is attributed to this region which is smaller than its saturation value s_a^*. These values are treated as constants. We intend to include prognostic equations for these entropies in a refined model version. For the present low order model we only need to calculate the boundary layer mass flux from the ambient region into the eyewall region. By Eq. (4) it does not only depend upon tangential wind v_{b2} and physical radius r_{b2} but also on absolute vorticity ζ_{b2}. To determine ζ_{b2} a wind profile in the vicinity of r_{b2} must be known. We assume the profile to be in the shape of

$$v_b = \frac{v_{b2} r_{b2}^{\beta}}{r^{\beta}} \quad \text{for} \quad r > r_{b2}, \qquad (11)$$

where the exponent β takes a value between 0.5 and 1. Consequently, the absolute vorticity ζ_{b2} at the outer eyewall boundary becomes

$$\zeta_{b2} = f + (1-\beta)\frac{v_{b2}}{r_{b2}}. \qquad (12)$$

This expression can be substituted in Eq. (4) to determine the mass transport into the eyewall region. The mass transport turns out to be sensitive to changes in β. A theoretically determined value by Emanuel (1986) becomes β=0.542. For such a small value, however, the radial inflow to the eyewall region is too weak compared to simulations with more complex models. A maximum value of β=1 on the other hand results in an unrealistically

[2] Please note that the coarse assumption of a constant density does not have a large impact on the tangential wind v_b, as detected by Frisius (2005). Furthermore, the relation $r_{b2}^2 = (GH)^{-1}$ is almost satisfied for a fully developed tropical cyclone so that the assumptions of mass conservation and constant density are irrelevant in this regime.

high radial wind even larger than the tangential wind.

2.4 THE THERMODYNAMIC EQUATIONS

The low order model is based upon thermodynamic variables. All needed hydrodynamic variables can be deduced diagnostically from Eqs. (7), (9), (10), (12) and (4). First, a prognostic equation for saturation entropy of the eyewall s_i* is needed. It is changed by the mass flux from the boundary layer and diabatic processes like radiation or turbulent mixing. The mass flux results from (4) evaluated at $r=r_{b2}$. The mass of the eyewall region itself is given by:

$$M_i = \pi\rho \int_{H_b}^{H+H_b} r_2^{\,2} - r_1^{\,2} dz = M - \pi\rho H r_1^{\,2} \,, \qquad (13)$$

and is treated as a constant. The diabatic processes are parameterized with a linear relaxation to a reference state that is set to zero by convention. Furthermore, we assume saturation so that we can equate entropy with saturation entropy. Then, we obtain the following prognostic equation

$$\frac{ds_i^{\,*}}{dt} = \psi_{b2} \frac{s_{bi} - s_i^{\,*}}{M_i} - \frac{s_i^{\,*}}{\tau_E} \,, \qquad (14)$$

where s_{bi} is the specific entropy of the boundary layer beneath the eyewall and τ_E the time scale for damping by diabatic cooling processes.

Further equations for specific entropy of the boundary layer are needed. To calculate their tendencies, the mass of the boundary layer beneath the eyewall must be known. It is given by

$$M_{bi} = \pi\rho_b (r_{b2}^{\,2} - r_{b1}^{\,2}) H_b \qquad (15)$$

and may change in the course of the development due to a change in r_{b2}. The specific entropy is altered by: surface heat fluxes, lateral inflow and diabatic cooling. These are applied by the following equation

$$\frac{ds_{bi}}{dt} = \psi_{b2} \frac{s_{ba} - s_{bi}}{M_{bi}} + \frac{C_H}{2H_b} |v_{b2}| (s_O - s_{bi}) - \frac{s_{bi}}{\tau_E} \,, \qquad (16)$$

where s_{ba} denotes the mean specific boundary layer entropy beneath the ambient region, C_H the surface transfer coefficient for entropy and s_O the specific entropy at the ocean surface. The factor ½ is introduced to account for the decrease in wind speed from v_{b2} to a smaller value towards the centre of the storm.

The specific boundary layer entropy s_{ba} beneath the ambient region is altered by surface heat fluxes, diabatic cooling and downwelling of low-entropy air from the free atmosphere above the boundary layer. Therefore, the prognostic equation for s_{ba} takes the form

$$\frac{ds_{ba}}{dt} = \psi_{b2} \frac{s_a - s_{ba}}{M_{ba}} + \frac{C_H}{2H_b} |v_{b2}| (s_O - s_{ba}) - \frac{s_{ba}}{\tau_E} \,, \qquad (17)$$

where $M_{ba}=\pi\rho_b(r_{ba}^{\,2}-R_2^{\,2})H_b$ is a characteristic boundary layer mass. The radius r_{ba} can be interpreted as the outer radius of the ambient boundary layer and determines the strength of the entrainment of the overlying air, which possesses a relatively low specific entropy s_a.

Finally, we must determine the specific entropy s_O at the sea surface since it changes with time due to its dependence on surface pressure p_s. We use the approximated expression

$$\begin{aligned} s_O(T_s, p_s) &= c_p \ln(T_s / T_{ref}) - R_d \ln(p_s / p_{ref}) \\ &+ L_v \left(\frac{q_v^{\,*}}{T_s} - \frac{q_{vref}}{T_{ref}} \right) , \end{aligned} \qquad (18)$$

where T_s denotes the sea surface temperature and q_v the specific humidity. The index *ref* symbolizes that the quantity is a constant reference quantity and the asterisk denotes that the moisture variable is considered at saturation. The reference entropy s_{ref} coincides with the boundary layer entropy of the undisturbed environment. Here, the temperature is identical to the sea surface temperature T_s (SST) and the relative humidity takes the value h_{ref}. Therefore, we obtain

$$s_O = -R_d \ln(p_s / p_{ref}) + L_v \left(\frac{q_v^{\,*} - h_{ref} q_{v,ref}^{\,*}}{T_s} \right). \qquad (19)$$

We assume gradient wind balance to calculate the surface pressure p_s. Hence

$$\frac{R_d T_s}{p_s} \frac{\partial p_s}{\partial r} = \frac{v_b^{\,2}}{r} + f v_b \,, \qquad (20)$$

where R_d is the specific gas constant. A radial integration to infinity would lead to a diverging integral when the tangential wind takes a profile of the shape described by Eq. (11). Therefore, the integration is only applied to a finite radius r_a where the surface pressure coincides with the reference value. By integration of Eq. (20) we obtain

$$\begin{aligned} &R_d T_s \ln(p_{s2} / p_0) = \\ &= -\frac{v_{b2}^{\,2}}{2\beta} \left[1 - \left(\frac{r_{b2}}{r_a} \right)^{2\beta} \right] + \frac{f v_{b2} r_{b2}}{1-\beta} \left[1 - \left(\frac{r_a}{r_{b2}} \right)^{1-\beta} \right]. \end{aligned} \qquad (21)$$

The surface pressure can be used to evaluate the entropy s_O at the radius r_{b2} where Eqs. (16) and (17) are evaluated.

Note that the convective-radiative equilibrium state is neutral to convective instability. Consequently, the entropy values are relaxed to zero by the damping terms in Eqs. (14), (16) and (17). For consistency the specific saturation entropy s_a* of the ambient region is set to zero. The actual entropy s_a however, is smaller than s_a* due to sub-saturation. It is given by the formula

$$s_a = L_v \frac{q_v(T_a, p_a, h_a) - q_v^{\,*}(T_a, p_a)}{T_a} , \qquad (22)$$

where the index a denotes that the quantity is evaluated in the ambient region at a characteristic pressure level above the boundary layer. The temperature T_a is determined by a moist-adiabatic parcel displacement to the pressure level p_a where saturation of the parcel is assumed.

2.4 THE DYNAMICAL SYSTEM

The low order model takes the form of a dynamical system with three autonomous ordinary differential equations for the three unknowns s_i*, s_{bi} and s_{ba}. The equations are given by

$$\frac{ds_i^*}{dt} = \psi_{b2}\frac{s_{bi}-s_i^*}{M_i} - \frac{s_i^*}{\tau_E},$$
$$\frac{ds_{bi}}{dt} = \psi_{b2}\frac{s_{ba}-s_{bi}}{M_{bi}} + \frac{C_H}{2H_b}|v_{b2}|(s_O - s_{bi}) - \frac{s_{bi}}{\tau_E},$$
$$\frac{ds_{ba}}{dt} = \psi_{b2}\frac{s_a-s_{ba}}{M_{ba}} + \frac{C_H}{2H_b}|v_{b2}|(s_O - s_{ba}) - \frac{s_{ba}}{\tau_E}. \quad (23)$$

In these equations the mass stream function ψ_{b2}, the tangential velocity v_{b2} and the specific entropy at the sea surface s_O can be written as a function of s_i* by consideration of Eqs. (4), (10), (12) and (21). This is advantageous for the calculation of equilibria since we can derive a single equation for the equilibrium values of s_i*.

The system dynamics depend on a number of model parameters. These are M, M_i, r_a, r_{ba}, r_{b1}, τ_E, C_H, C_D, H, H_b, f, R_2, ΔR, ρ, ρ_b, Γ, T_s, h_a, p_a, h_{ref}, p_{ref} and β.

3. MODEL RESULTS

As a standard parameter set of our model experiments we use the following values:

r_a=r_{ba}=400km, R_2=300km, ΔR=30km, r_{b1}=10km, H_b=2km, H=10km, ρ=0.5kg/m^3, ρ_b=1.1kg/m^3, C_H=C_D=0.003, τ_E=18h, f=0.5×10^{-4}s^{-4}, Γ=0.0065K/m, h_a=70%, h_{ref}=70%, p_a=750hPa, p_{ref}=1000hPa and β=0.875.

Simulations are based on this set, unless stated otherwise. The mass M coincides with that of the state at rest, i.e.:

$$M = \pi\rho_b R_2^{\,2} H\,. \quad (24)$$

First, equilibria are determined by an iterative procedure. The output of the standard simulation with gradual change in sea surface temperature (SST) shows three equilibria. The first one is associated with an atmosphere at rest, the second one with a low pressure system of small intensity and the third one with a tropical cyclone. Conducting a stability analysis by which eigenvalues from the respective Jacobi matrix are numerically determined, we detect that the equilibria of an atmosphere at rest and of a tropical cyclone are stable while the intermediate equilibrium is unstable. Figure 2 displays the maximum tangential wind of these equilibria as a function of SST for various values of the profile parameter β. Obviously, the upper two equilibria arise after a subcritical bifurcation at a SST close to 5℃. The intensity of the tropical cyclone increases with SST as expected while that of the unstable solution decreases. There is also an increase of tropical cyclone intensity with β. This result stems from an intensification of the boundary layer inflow due to a decline in vorticity (see Eqs. (4) and (12)). For β=0.875 an inflection point arises in the tropical cyclone branch. This is related to a cusp catastrophe to be discussed below.

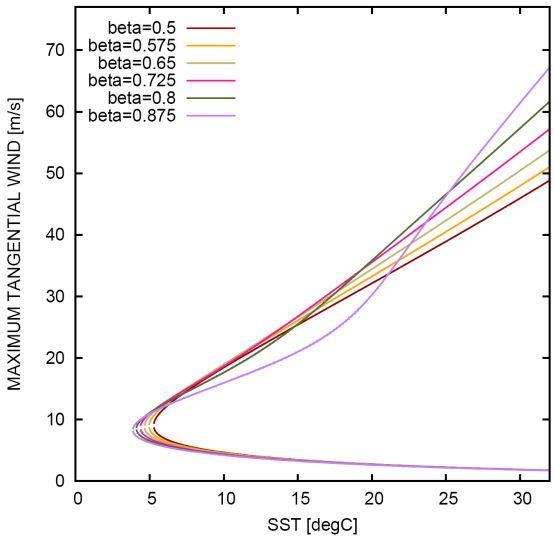

Figure 2: Bifurcation diagram of maximum tangential wind as a function of SST for different β values.

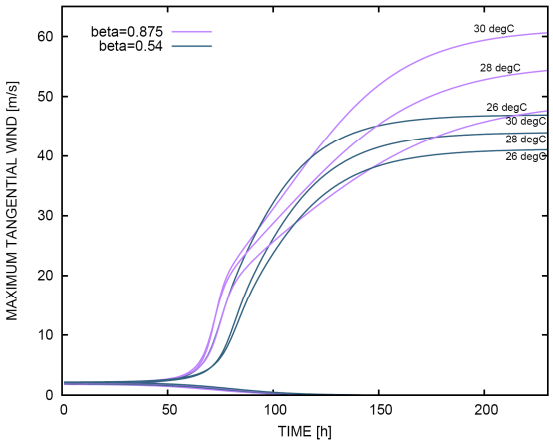

Figure 3: Time development of maximum tangential wind started near the unstable equilibrium at different SSTs (26°C, 28°C and 30°C) for β=0.54 (dark-blue lines) and β=0.875 (purple lines).

The repulsing effect of the unstable intermediate equilibrium leads to a threshold for cyclogenesis. It can be anticipated that tropical cyclogenesis only occurs in the model in cases where the initial intensity exceeds the one of the unstable equilibrium. This can be seen in Figure 3, which shows the time development of maximum tangential wind for two initial conditions near the repulsing equilibrium and

at different SSTs observable in tropical regions and two different β values, one of which is very close to that proposed by Emanuel (1986). It becomes evident that the unstable equilibrium defines a threshold and leads to a finite amplitude nature of tropical cyclogenesis in the model. This result is consistent with the observed fact that not all tropical depressions transform into tropical cyclones. Furthermore, the results show that the amplitude threshold decreases with increasing temperature.

The equilibria are also sensitive to parameters determining the entrainment of low-entropy air in the ambient region. Equilibrium solutions for a SST of 28°C as a function of relative humidity h_a and outer radius r_{ba} are displayed in Fig. 4. It shows that two additional equilibria arise at low relative humidity and small outer radii due to a cusp catastrophe that occurs for intermediate values of both parameters. The lower one of the two additional equilibria forms another stable solution that can be associated with a tropical depression. Therefore, tropical cyclogenesis is very unlikely in this regime. The cusp catastrophe is less pronounced at smaller β (Fig. 4B) since reducing β results in a weaker radial inflow.

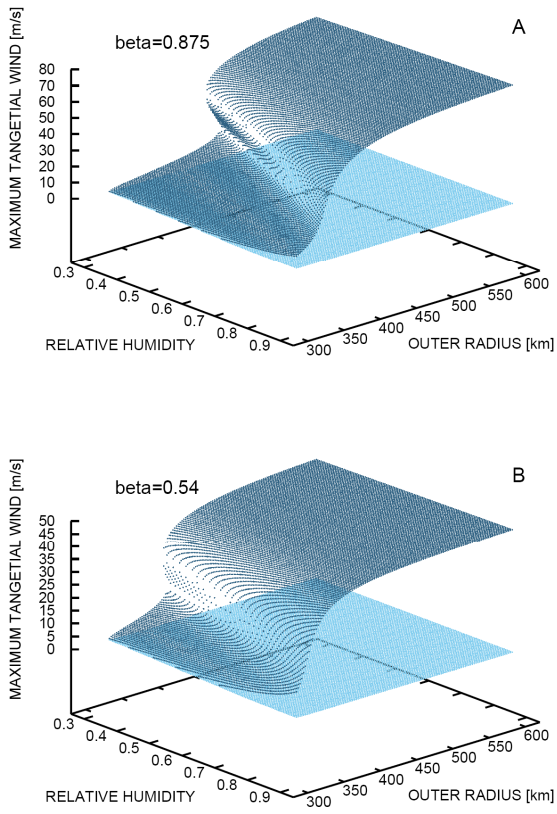

Figure 4: Equilibrium solutions for maximum tangential wind as a function of relative humidity h_a and outer boundary layer radius r_{ba} for: (A) β=0.875 and (B) β=0.54.

The entrainment effect also affects the dependence of equilibrium solutions on SST. This is displayed in Fig. 5 showing the equilibria as a function of SST and relative humidity h_a. It becomes evident that relative humidity exerts a strong impact on the equilibria at an outer radius of 400km and β=0.875 (Fig. 5A). Obviously, the four equilibria occur for SSTs typical of tropical oceans and a relative humidity between 60% and 70%. Therefore, tropical cyclogenesis becomes impossible for smaller relative humidity in this model regime. Instead, non-developing tropical depressions may form. Furthermore, the cusp catastrophe is related to a SST threshold for development in a certain relative humidity range. The SST profile along a relative humidity of 63% indeed displays the bifurcation leading to the four equilibria at a SST of 27°C. If this bifurcation is relevant to the observed SST threshold for tropical cyclogenesis remains unclear and still needs further investigation.

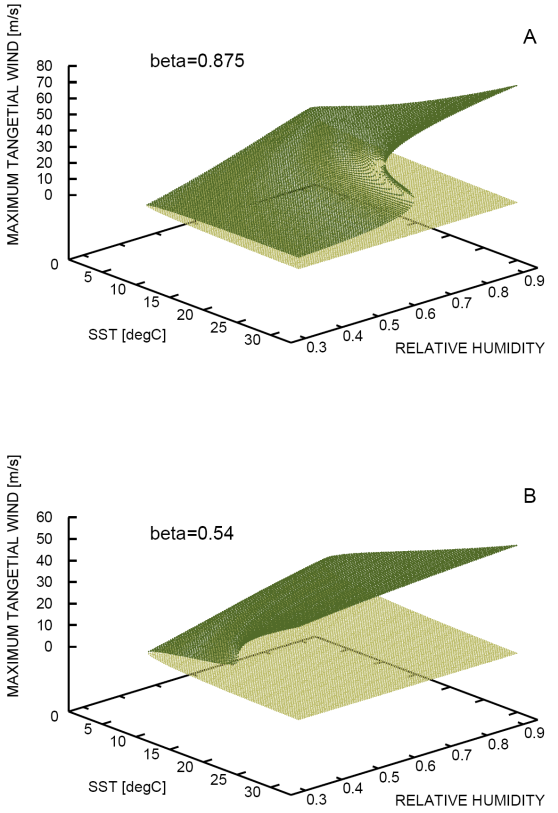

Figure 5: Equilibrium solutions for maximum tangential wind as a function of SST and relative humidity h_a for: (A) β=0.875 and (B) β=0.54.

4. CONCLUSIONS

The three region low order model of a tropical cyclone displays bifurcation characteristics in agreement with Emanuel and Nolan (2004). The equilibria are formed by one unstable and two stable branches. Two of them arise after a saddle node bifurcation above a critical threshold temperature. The repulsive property of the unstable equilibrium explains why some initial model depressions develop and others do not. Furthermore, it was found that relative humidity in the ambient region has an important qualitative impact on the system dynamics. Within a certain relative humidity range depending on β, two additional equilibria arise by a cusp catastrophe. These form a large obstruction for tropical cyclone formation and can be explained by the entrainment of low-entropy air into the subcloud boundary layer. Previous studies also point to the

importance of mid-tropospheric moisture content for tropical cyclogenesis in reality (e.g. DeMaria et al. 2001). Moreover, our results are consistent with findings by Emanuel (1989, 1995) based on a more complex but still simplified model. A similar effect by low-entropy air import has been found in complex non-hydrostatic tropical cyclone models by Frisius and Hasselbeck (2009). They related the existence of downdrafts to latent cooling.

The dynamical system characteristics of the present model depend crucially on the existence of damping terms, which we have not specified so far. They can be associated with radiative cooling and turbulent and convective exchange in radial and vertical direction. An investigation of the role of these various processes can only be carried out using a more complex model. Therefore, we intend to perform a bifurcation analysis with the non-hydrostatic axisymmetric model HURMOD (for details see Frisius and Hasselbeck, 2009). In this model it is possible to detect steady state solutions when latent cooling processes are ignored. Identifying maximum wind speed of such a solution as a function of SST exhibits a curve similar to the upper stable branch displayed in Figure 2 (not shown).

With the dynamical system approach we also expect a better understanding of maximum potential intensity (MPI) of tropical cyclones. In the low order model many parameters influence the intensity and it is not obvious that existing MPI theories are consistent with the model we present here. Therefore, more detailed investigations with the low order model as well as with more complex models will be carried out in the future to gain more insight in MPI.

5. ACKNOWLEDGEMENT

This work was supported by the DFG within the Cluster of Excellence 177 Integrated Climate System Analysis and Prediction (CliSAP).

REFERENCES

DeMaria, M., J. A. Knaff, and B. H. Connell, Bernadette H., 2001: A tropical cyclone genesis parameter for the tropical Atlantic. *Weather and Forecasting*. **16**, 219-233.

Emanuel, K. A., 1986: An air-sea interaction theory for tropical cyclones. Part I: Steady-state maintenance. *J. Atmos. Sci.,* **43,** 585-604.

Emanuel, K. A., 1989: The finite-amplitude nature of tropical cyclogenesis. *J. Atmos. Sci.,* **46**, 3431-3456.

Emanuel, K. A., 1995: The behaviour of a simple hurricane model using a convective scheme based on subcloud-layer entropy equilibrium. *J. Atmos. Sci.*, **52**, 3960-3968.

Emanuel, K. A., and D. S. Nolan, 2004: Tropical cyclone activity and the global climate system. Extended abstract. The 26th Conference on Hurricanes and Tropical Meteorology.

Frisius, T., 2005: A balanced model of an axisymmetric vortex with zero potential vorticity. *Tellus*, **57**, 55-64.

Frisius, T., 2006: Axisymmetric tropical cyclogenesis via a single convective ring. Extended abstract. The 27th Conference on Hurricanes and Tropical Meteorology (Monterey, CA).

Frisius, T., and T. Hasselbeck, 2009: The effect of latent cooling processes in tropical cyclone simulations. *Quart. J. Roy. Meteor. Soc.*, **135,** 1732-1749.

Schubert, W. H. and J. J. Hack, 1983: Transformed Eliassen balanced vortex model. *J. Atmos. Sci.,* **40**, 1571-1583.

Smith, R. K., and M. T. Montgomery, 2008: Balanced boundary layers used in hurricane models. *Quart. J. Roy. Meteor. Soc.*, **134**, 1385-1395.